

A simulation- and model-based approach to PI control pairing and tuning for the pyro process in a cement plant

Jan Lorenz Svensen* Steen Hørsholt*
Guruprasath Muralidharan** John Bagterp Jørgensen*,***

* 2-control ApS, DK-7400 Herning, Denmark

** Ramco Industrial Technology Services, IN-600004 Chennai, India

*** Technical University of Denmark, DK-2800 Kgs Lyngby, Denmark

Abstract: The operation of the pyro process in cement production significantly affects the energy efficiency and sustainability of the cement plant, especially for reductions in carbon dioxide emissions. Hence, pyro process control is essential to obtain efficient and sustainable operation of cement plants. In this paper, we demonstrate how simulations and models can be utilized to evaluate and design control strategies for the pyro section in cement plants. We apply a novel differential algebraic equation (DAE) model for dynamic simulation of the pyro-section in cement plants to design decentralized PI controllers for the pyro-section. We utilize the pyro-process model to evaluate the control structure design. Through linearization of the pyro-process model, we apply the Relative Gain Array (RGA) method to choose and evaluate the pairings of the manipulated variables (MVs) and the controlled variables (CVs). Using simulations of the pyro-section, we generate step responses to estimate transfer models and apply Internal Model Control (IMC) for the tuning of the individual decentralized single-input single-output (SISO) PI controllers. Closed-loop simulations of the PI controllers demonstrate that PI controllers with IMC parameters provide smoother and faster responses compared with manually tuned PI parameters.

Keywords: Cement pyro section control, PID control, DAE model, IMC-based tuning, RGA

1. INTRODUCTION

Cement plants constitute a vital part of the construction industry and infrastructure of modern civilization. However, they are responsible for 8% of global CO₂ emissions (Lehne and Preston, 2018). Thus, improving the balance between economic progress and environmental responsibility is important when using cement for highways, bridges, and cities. To move towards zero CO₂ emission cement plants, a first step is to apply advanced process control (APC) for more efficient operation of existing cement plants, while further steps may be to modify the process and reduce the clinker dependence or capture and store the CO₂ produced in the cement manufacturing process. Traditional cement is primarily made of clinker. The production of clinker involves mining, blending, grinding, and pyro processing the raw materials. The pyro-process is the main source of emissions and energy consumption. Research has studied several alternative strategies (Ram-samy et al., 2023), including changing parts of the overall process, such as using electrification and carbon capture (Varnier et al., 2025).

A range of advanced control strategies for cement plants have been implemented and documented. These include fuzzy logic control (Holmblad and Østergaard, 1993), rule-based neural network control (Bo et al., 1997), and

model predictive control (MPC). MPC applications include Stadler et al. (2011), Zanoli et al. (2015a,b, 2023), Teja et al. (2016) for kiln and cooler control, Zhang et al. (2021, 2022) for raw meal blending and grinding, Muralidharan and Jørgensen (2009) and Muralidharan et al. (2010, 2013) for soft constrained based robust MPC of cement mills, and Huusom et al. (2005) for predictive control motivated physically based models of cement grinding units. Several models have been proposed to describe the processes. Spang (1972) described a reaction-based dynamic kiln model. Westerlund (1981) provided insight into data-based kiln models using ARMAX models. Noshirvani et al. (2009) suggested both Box-Jenkins models and neural-network models. Stadler et al. (2011) proposed a mass-based dynamic kiln model. Melitos et al. (2025) suggested a steady-state pyro-process model. Svensen et al. (2024a,b, 2025a,b,c) provided dynamic models for each process section and a full pyro process model.

This work focuses on the pyro process shown in Figure 1. The pyro process consists of a preheating tower with five cyclones and calciner, a kiln, and a cooler. The start-up, shut-down, and operation of the pyro process is complicated and expensive. Any lost production or off-spec product is associated with a large economic penalty. Therefore, testing new control strategies and performing identification experiments (say step response tests) are often not allowed without detailed justification of the risks and benefits. A high-fidelity simulator can provide such

* Corresponding author: J.B. Jørgensen (e-mail: jbj@dtu.dk)

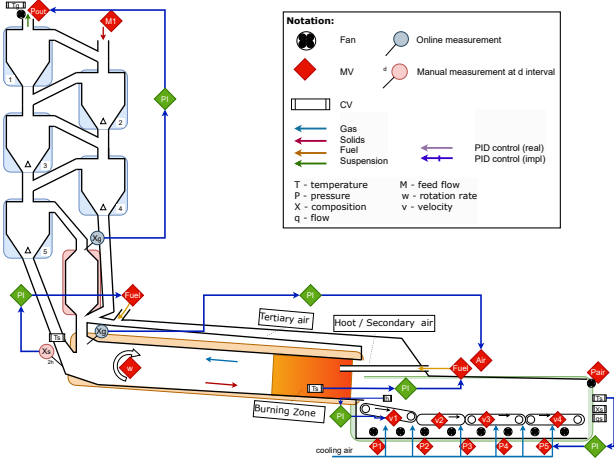


Fig. 1. a 5-stage pyro process with PI-control loops for cement production.

justification. We demonstrate the simulator for model-based PI-controller tuning and control structure selection. Such model-based PI-pairing and tuning for the pyro-process in a cement plant is novel.

This paper is organized as follows. Section 2 presents the pyro process, Section 3 describes the IMC control design, Section 4 presents the RGA analysis, and Section 5 provides the conclusions.

2. SYSTEM AND SIMULATOR

Figure 1 illustrates the layout of the pyro process in cement clinker production. It is a 5-stage single-string plant, meaning that the preheating tower contains 5 separation cyclones in series.

The raw meal enters near the top of the preheater. On its course through the preheater and calciner, it is heated and calcination occurs. In the kiln, the meal is heated to around 1300-1500°C at which it reacts chemically to form the different compounds of cement clinker. Lastly, the clinker passes through the cooler, where it is cooled rapidly to around 100°C to stabilize the products.

In the cooler, cooling air is partially circulated back into the process. The first part of the recirculation air flow, the secondary air, is sent to the kiln. The next part, the tertiary air, is sent to the calciner, while the rest escapes to the environment. In the kiln, the secondary air is mixed with the fuel-primary air mixture. Thus, fuel combustion and this recirculated heat provide the heat for the kiln reactions. In the calciner, the kiln gas is mixed with the tertiary air and additional fuel. This heats the feed and facilitates the main part of calcination. The gas flows up through the preheating tower and transfers its heat to the solid feed that flows down.

We use the simulation model described by Svensen et al. (2025c). The mathematical model is a differential-algebraic system consisting of 755 differential equations and 157 algebraic equations in the form:

$$\dot{x} = f(x, y, u, d, \theta_f), \quad (1a)$$

$$0 = g(x, y, u, d, \theta_g), \quad (1b)$$

$$z = h(x, y, u, d, \theta_h). \quad (1c)$$

x are the differential states, y is the algebraic states, u is the manipulated variables (MVs), d is the disturbances, z are the controlled variables (CVs), and θ are the model parameters. The DAE model includes thermo-physical properties, mass and energy transport, reaction stoichiometry and kinetics, and mass and energy balances with appropriate thermodynamic closures.

The MVs are

$$u = [P_{ph} F_{f,Ca} F_{f,K} F_{1st} F_{cool} v_{grate}]^T. \quad (2)$$

P_{ph} is the fan-induced pressure above the preheating tower, $F_{f,Ca}$ is the fuel mass flow going into the calciner, $F_{f,K}$ is the fuel mass flow going into the kiln, F_{1st} is the primary air mass flow send into the kiln with the kiln fuel, F_{cool} are cooling air flow injected below the grate belt of the cooler, and v_{grate} are the grate belt velocities. For simplicity, the F_{cool} fluxes and v_{grate} velocities are assumed identical across the cooler length.

The CVs are

$$z = [X_{O2,Ca} X_{CaO} X_{O2,K} T_{s,burn} T_{clinker} h_{bed}]^T. \quad (3)$$

$X_{O2,Ca}$ and $X_{O2,K}$ are the mole fraction of O_2 at the calciner outlet and kiln inlet, respectively. X_{CaO} is the calcination degree of the feed at the kiln inlet. $T_{s,burn}$ is the clinker temperature in the burning zone of the kiln. $T_{clinker}$ is the clinker temperature exiting the cooler, and h_{bed} is the height of the clinker bed in the cooler.

Using the Jacobians of the DAE model (1) at steady-state, a standard linear state space model, (A, B, C, D) , for the DAE model (1) is obtained by

$$A = \partial_x f - \partial_y f [\partial_y g]^{-1} \partial_x g, \quad (4a)$$

$$B = \partial_u f - \partial_y f [\partial_y g]^{-1} \partial_u g, \quad (4b)$$

$$C = \partial_x h - \partial_y h [\partial_y g]^{-1} \partial_x g, \quad (4c)$$

$$D = \partial_u h - \partial_y h [\partial_y g]^{-1} \partial_u g. \quad (4d)$$

The corresponding transfer function, $G(s)$, is computed by

$$G(s) = C(sI - A)^{-1} B + D. \quad (5)$$

3. CONTROL AND STEP RESPONSES

We design decentralized PI controllers using a manual trial-and-error tuning method for each PI-parameter as well as by using the simplified IMC (SIMC) tuning method (Skogestad, 2003). Both type of PI-controllers are simulated as continuous-time controllers that are implemented with limits but without anti-windup.

The manual tuning approach is included to illustrate the usage of the simulator as a digital twin for controller tuning and evaluation. The SIMC tuning approach highlights the benefits of using the simulator to provide data for model based control design.

The SIMC tuning approach needs a transfer function model for each (MV-CV) pair in the control structure. We simulate 4 sets of step responses to generate the data to estimate the models. The steps were sampled 100 times an hour (i.e. the sampling time is 36 seconds) with steps of $\pm 1\%$ and $\pm 0.5\%$ of steady-state control for each input. Figure 2 shows the CV step responses obtained for steps in the MVs. The manual chosen MV-CV control pairs are in the diagonal. Figure 3 shows the normalized responses.

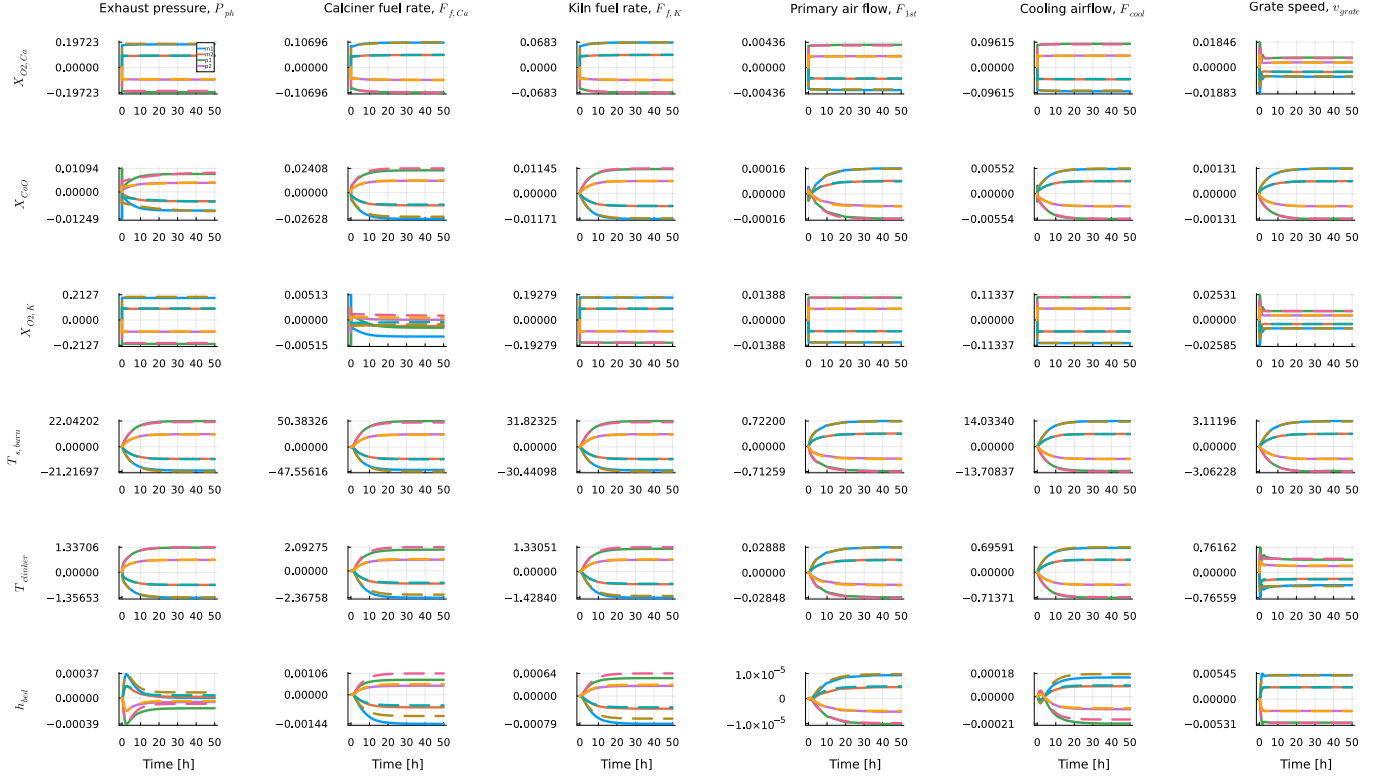


Fig. 2. MV-CV step responses: simulated step responses of the simulator for 4 different step sizes (m1: -1%(blue), m2: -0.5%(red), p1: 1%(green), p2: 0.5%(purple)) and step responses of the estimated model (dashed lines). Each row shows a CV's centered response to the MVs of each column.

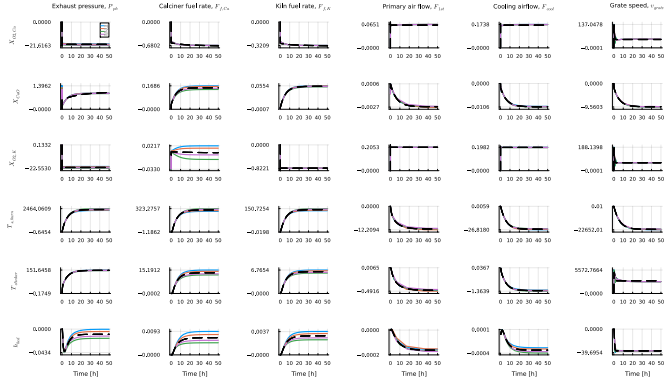


Fig. 3. MV-CV normalized step responses for 4 different step sizes (m1: -1%(blue), m2: -0.5%(red), p1: 1%(green), p2: 0.5%(purple)) and estimated model (dashed lines).

3.1 Transfer function estimation

Given the shape of the responses in Figure 2 and Figure 3, the data is fitted to a second-order transfer function,

$$Z_i(s) = \hat{G}_{ij}(s)U_j(s), \quad \forall i \times j \in CV \times MV, \quad (6)$$

$$\hat{G}_{ij}(s) = K_{ij,0} \frac{\tau_z^{ij}s + 1}{(\tau_1^{ij}s + 1)(\tau_2^{ij}s + 1)} e^{-\tau_d^{ij}s}. \quad (7)$$

Figure 3 shows that for all but a few, the normalized responses show similar dynamic behaviors across the 4 step sizes. The stationary values settle in the same vicinity, with only one pair having shifting signs, ($F_{f,Ca}, X_{O_2,K}$). Given the results, we deem linear models to be a good

representation in this range as the nonlinear effects appear to be minimal.

For the estimation of the transfer functions, we normalize the data between the stationary periods t_0 and t_f ,

$$s_{ij}(t) = \frac{z_i(t) - z_i(t_0)}{u_j(t) - u_j(t_0)}, \quad (8)$$

such that $s_{ij,t}$ corresponds to $\hat{G}_{ij}(s)$. As $U(s) = 1/s$ is the unit step, the normalized step transfer function is

$$\bar{S}_{ij}(s) = \hat{G}_{ij}(s) \frac{1}{s}. \quad (9)$$

We fit the data to the time-domain equivalents of (9). The equivalent function depends on the values of τ_1 and τ_2 . Generally, the function is given by

$$\bar{s}_{ij}(t) = K_h \left(1 - \frac{\tau_z^{ij} - \tau_1^{ij}}{\tau_2^{ij} - \tau_1^{ij}} e^{-\frac{\Delta t}{\tau_1^{ij}}} - \frac{\tau_z^{ij} - \tau_2^{ij}}{\tau_2^{ij} - \tau_1^{ij}} e^{-\frac{\Delta t}{\tau_2^{ij}}} \right), \quad (10)$$

but in the case of $\tau_1 = \tau_2$, it is given as

$$\bar{s}_{ij}(t) = K_h \left(1 - \left(1 + \Delta t \frac{\tau_1^{ij} - \tau_z^{ij}}{(\tau_1^{ij})^2} \right) e^{-\frac{\Delta t}{\tau_1^{ij}}} \right). \quad (11)$$

$\Delta t = t - \tau_d^{ij}$ is the time offset and $K_h = K_{ij,0}H_d$ is a delayed gain, where $H_d = H(\tau_{ij},d)$ is the heavy-side function. Figure 2 and Figure 3 show the step responses of (1) and of the estimated transfer functions (dashed lines), which clearly fit the data. Initial guesses for the stationary gain and delay can be determined by

$$K_{ij,0} = s_{ij}(t_f), \quad (12)$$

and by evaluating the earliest change:

$$\tau_d^{ij} : |s_{ij}(\tau_d^{ij})| > \epsilon, \quad \epsilon = 10^{-10}. \quad (13)$$

Table 1. Estimated transfer functions for the (MV-CV) pairs in the decentralized control structure. τ is in seconds.

MV	CV	K_0	τ_1	τ_2	τ_z	τ_d
P_{ph}	$X_{O_2, Ca}$	-20.54	7.93	7.93	21.74	0.18
$F_{f, Ca}$	X_{CaO}	0.29	9.23	18103.3	3663.1	0.04
$F_{f, K}$	$T_{s, burn}$	103.35	2153.3	19191.9	1187.8	162.02
F_{1st}	$X_{O_2, K}$	0.26	2.64	16.4	32.07	0.024
F_{cool}	$T_{clinker}$	-4.75	1001.1	20072.9	2694.2	1073.9
v_{grate}	h_{bed}	-36.88	969.2	969.2	-0.38	920.3

The (MV-CV) pairs in the decentralized PI-control structure are $(P_{ph}-X_{O_2, Ca})$, $(F_{f, Ca}-X_{CaO})$, $(F_{f, K}-T_{s, burn})$, $(F_{1st}-X_{O_2, K})$, $(F_{cool}-T_{clinker})$, and $(v_{grate}-h_{bed})$. Exhaust pressure and primary air control local O_2 levels through the air flows. Fuel rates regulate local process conditions, i.e. the calcination degree and the clinker burner temperature. Cooling air regulates the clinker cooling process i.e. the clinker temperature. The grate belt velocity regulates bed height to ensure flow uniformity.

Table 1 shows the estimated parameters for the transfer functions corresponding to the (MV-CV) pairs in the decentralized control structure.

3.2 IMC

The design of the PI-controller using IMC design (Skogestad, 2003), relies on approximating the general transfer function,

$$G_0(s) = k_0 \frac{\prod_i^{n_z} (\tau_{z,i}s + 1)}{\prod_i^{n_p} (\tau_{p,i}s + 1)} e^{-\tau_d s}, \quad (14)$$

$$\tau_{k,i} \geq \tau_{k,j} \quad \text{for } i \geq j \quad \text{and } k \in \{z, p\},$$

into a first-order system,

$$G_1(s) = \frac{k}{\tau_1 s + 1} e^{-\tau_d s}. \quad (15)$$

The IMC rules for the approximation depend on the sign of the zeros, τ_z . For positive τ_z , the rules approximate a zero-pole fraction,

$$\frac{\tau_z s + 1}{\tau_p s + 1}, \quad (16)$$

as a gain scaling and/or replacement pole. When each positive τ_z is approximated, the effective delay τ_d and the first-order poles are computed from the remaining poles, zeros, and delay.

$$\tau_1 = \tau_{p,1} + \frac{\tau_{p,2}}{2}, \quad (17)$$

$$\tau_d := \tau_d + \frac{\tau_{p,2}}{2} + \sum_{j=3}^{n_p} \tau_{p,j} - \sum_{i \in \tau_{z,i} \leq 0} \tau_{z,i}. \quad (18)$$

The PI gains are then computed by

$$K_P = \frac{1}{k} \frac{\tau_1}{\tau_c + \tau_d}, \quad K_I = \frac{K_P}{\min(\tau_1, 4(\tau_c + \tau_d))}, \quad (19)$$

with $-\tau_d < \tau_c < \infty$. In the tuning, we use the standard recommendation of $\tau_c = \tau_d$ as our initial parameter. We kept this tuning in the controllers $(P_{ph}-X_{O_2, Ca})$, $(F_{f, K}-T_{s, burn})$, and $(F_{cool}-T_{clinker})$, while τ_c was further adjusted in the remaining control loops. Table 2, shows the PI gains (K_P and K_I) and τ_c for each pairing.

Figure 4 shows the CVs, the MVs, and selected process KPI values for simulations with the PI controllers with

Table 2. Pairings and parameters for the decentralized PI-controllers with manual tuning and IMC-based tuning. τ_c is in seconds.

MV	CV	K_P		K_I		τ_c
		IMC	Manual	IMC	Manual	
P_{ph}	$X_{O_2, Ca}$	-0.0089	-0.01	-0.006	-0.001	0.18
$F_{f, Ca}$	X_{CaO}	12.51	0.005	1.35	0.011	10.0
$F_{f, K}$	$T_{s, burn}$	0.47	0.07	3.6e-4	1.4e-5	162.02
F_{1st}	$X_{O_2, K}$	0.014	0.008	0.0069	0.16	0.5
F_{cool}	$T_{clinker}$	-0.32	-2.8e-4	-3.2e-4	-2.8e-4	1073.9
v_{grate}	h_{bed}	-0.097	-0.02	-6.7e-5	-0.0001	-1000.0

manual tuning and IMC-based tuning. Figure 5 is the same simulations during the first 5 hours. Figures 4 and 5 show that the IMC tuned decentralized PI-controller provides an overall smoother and faster operation than the manually tuned decentralized PI-controller. The burner temperature and calcination degree settle fast for the IMC-PI, while the manually tuned PI takes several hours to settle. The responses are also more similar to first/second-order responses than for the manually tuned PI. We also see that given the primary air's less integral action, it does not reach saturation, allowing the other PIs to settle without a sudden change when the saturation finishes.

This gives a good demonstration of how access to a simulator model can improve control design and tuning for the cement process.

4. RGA

In this section, we utilize the model to evaluate the control structure. The pairing of MVs and CVs in the decentralized PI controller can be evaluated using the relative gain array (RGA) method described by Jørgensen and Jørgensen (2000) and Skogestad and Postlethwaite (2005).

The RGA method computes a matrix, Λ from a transfer function matrix G at a given frequency ω ,

$$\Lambda_\omega(G) = G(i\omega) \circ (G(i\omega)^{-1})^T. \quad (20)$$

When $[\Lambda_\omega(G)]_{i,j} = 1$, the pairing is ideal. The pairing is usually evaluated using the relative interaction (RIA),

$$[\Phi_\omega]_{i,j} = \frac{1}{[\Lambda_\omega(G)]_{i,j}} - 1. \quad (21)$$

In the analysis, we apply a sequential evaluation of the pairings. At each step, we find the pairing with the minimum absolute relative interaction,

$$(i, j) = \arg \min(|\Phi_0|). \quad (22)$$

The corresponding row and column of the pair are removed from Φ_0 , and we repeat to find the next pair. Alternatively, one can minimize the sum of relative interactions by solving an assignment optimization problem (Jørgensen and Jørgensen, 2000).

Table 3 shows the RGA matrix, Λ_0 , evaluated at the steady-state frequency, $\omega = 0$. The clinker outflow, F_{clink} , and the raw meal feed inflow, F_{feed} , are appended to the CVs and MVs, respectively. Table 3 also shows the (MV-CV)-pairing for the simulations and the suggested pairing with the RGA/RIA method. In both cases, the grate belt speed and feed flow have the same pairs with almost ideal RGA value. As the remaining PI-loop pairs have high

¹ \circ : the schur product or element-wise multiplication

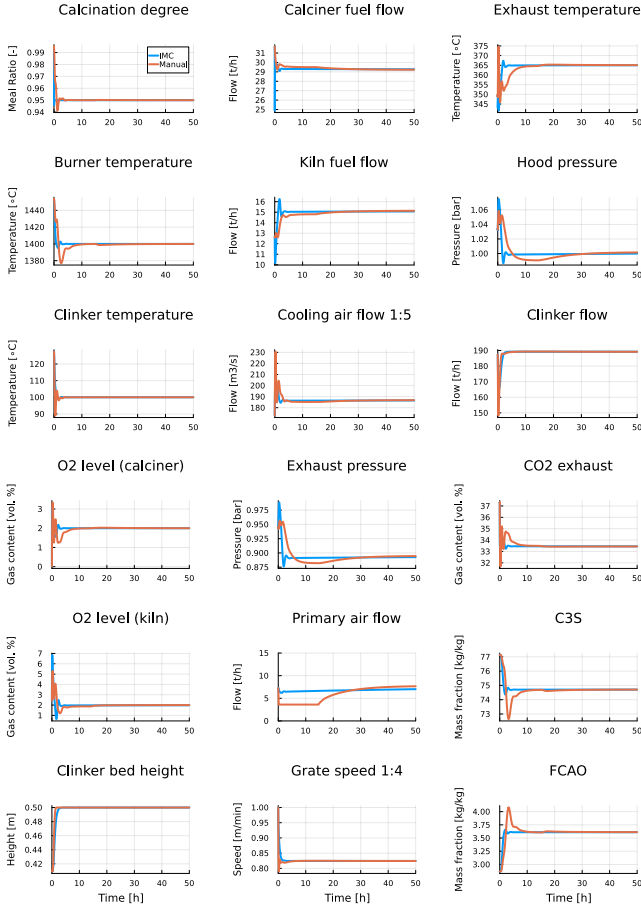


Fig. 4. 50-hour closed-loop simulations using the IMC-PI and the manually tuned PIs. The first column shows the CVs, the second column shows the MVs, while the third column shows KPIs of interest for the process, such as clinker content (C3S, FCAO [free lime]).

Table 3. RGA matrix. PI-loop pairs (blue,orange). RGA-based pairs (red,orange).

CV\MV	v_{grate}	P_{ph}	F_{feed}	$F_{f,Ca}$	$F_{f,K}$	F_{1st}	F_{cool}
$X_{O_2,Ca}$	-7e-6	5.20	-0.08	-1.13	1.61	-2.17	-2.43
X_{CaO}	1e-5	-6.62	1.30	13.4	-14.4	3.87	3.51
$X_{O_2,K}$	8e-5	-3.56	-0.02	-0.01	-4.23	7.14	1.69
$T_{s,burn}$	-0.01	8.54	-1.38	-11.7	19.4	-8.35	-5.51
F_{clink}	1e-3	-0.17	1.04	2e-3	0.01	0.04	0.08
$T_{clinker}$	-2e-6	-2.41	0.18	0.42	-1.26	0.45	3.61
h_{bed}	1.01	0.02	-0.04	0.02	-0.08	0.02	0.05

values, they are less ideal pairings than those provided by the RGA method. Though relatively, the $T_{clinker}-F_{f,Ca}$ pairing is worse than the $T_{clinker}-F_{cool}$ pair is.

If the uniform cooling air flow assumption is changed to 3 cooling air flow rates instead, the pairing changes to $(F_{feed}-F_{clink}, 0.90)$, $(F_{cool,1}-X_{O_2,Ca}, 1.05)$, $(P_{ph}-X_{CaO}, 1.11)$, $(F_{cool,2:3}-T_{s,burn}, 1.58)$, $(F_{1st}-X_{O_2,K}, 4.91)$, $(F_{cool,4:5}-T_{clinker}, 1.05)$, and $(v_{grate}-h_{bed}, 1.01)$. The extra inputs provide more ideal pairings, though the fuel flows are not in any pairs. The $T_{clinker}-F_{cool,4:5}$ pair is similar to the original cooling-flow pair used in the PI-loops, supporting the rationale for the initial choices.

Using the step response tests, we can illustrate the effective changes in each CV of the system against each MV.

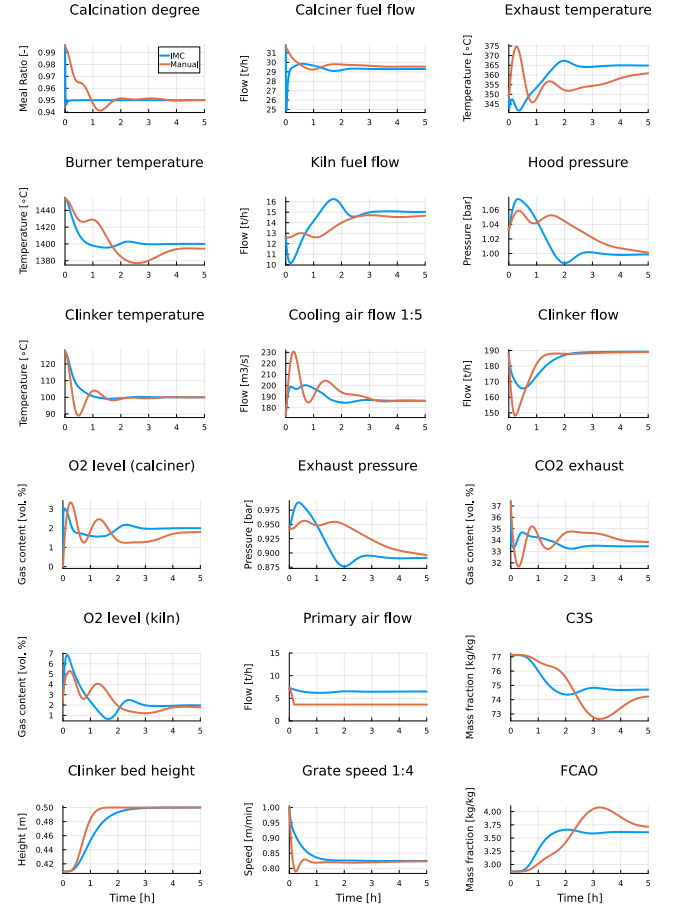


Fig. 5. The first 5 hours of the closed-loop simulations in Figure 4. Clarifying the faster settling of the IMC-PI. The columns show the CVs, MVs, and selected KPIs.

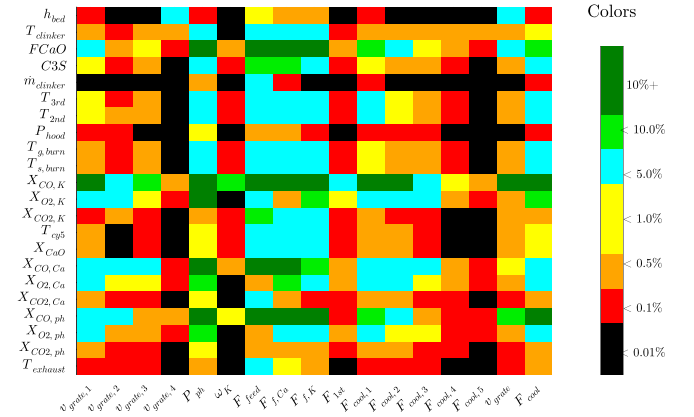


Fig. 6. Responsiveness of CVs to MVs. Maximum relative change of CVs to steps in the MVs. Colored by discrete percentage ranges.

Figure 6 shows the categorized percentage change of each step response. In the RGA above, $T_{s,burn}$ was paired with different MVs depending on the MVs available. Figure 6 shows that $T_{s,burn}$ is most impacted by P_{ph} , $F_{f,meat}$, $F_{f,Ca}$, $F_{f,K}$, and the cooling air. This fits with the initial pairing, $F_{f,K}$, and the first RGA pairing, P_{ph} . The second RGA pairing chooses a less changing pairing, thus a less sensitive interaction.

5. CONCLUSION

We used a simulation model for the pyro section in a cement plant to design and tune a decentralized PI controller. We demonstrated the use of the model to obtain linear models that are used for RGA-based control structure selection and IMC-based tuning. The linear models describe the process well in a small neighborhood around the steady state operating point. Such models are difficult to obtain in practical cement plant operation, but they can readily be obtained from a high-fidelity simulator. The paper is one step towards model-based design of controllers for cement plants. Future work considers the use of the identified linear model for model predictive control (MPC) design.

REFERENCES

- Bo, Y., Yi, L., and Shouning, Q. (1997). A rule-based cement kiln control systems using neural networks. In *IEEE International Conference on Intelligent Processing Systems*, 493–497.
- Holmblad, L.P. and Østergaard, J.J. (1993). Control of a cement kiln by fuzzy logic. In D. Dubois, H. Prade, and R.R. Yager (eds.), *Readings in Fuzzy Sets for Intelligent Systems*, 337–347. Morgan Kaufmann Publishers, Inc.
- Huusom, J.K., Jensen, A.D., Jørgensen, S.B., Michelsen, M., Knudsen, J., Recke, B., and Jørgensen, J.B. (2005). Modelling of cement grinding circuits for predictive control. *IFAC Proc. Vol.*, 38(1), 350–355.
- Jørgensen, J.B. and Jørgensen, S.B. (2000). Towards automatic decentralized control structure selection. *Computers & Chemical Engineering*, 24, 841–846.
- Lehne, J. and Preston, F. (2018). Making concrete change: Innovation in low-carbon cement and concrete. Technical report, Chatham House.
- Melitos, G., de Groot, B., and Bezzo, F. (2025). Model based flowsheet studies on cement clinker production processes. *Systems & Control Transactions*, 4, 153–158.
- Muralidharan, G. and Jørgensen, J.B. (2009). Soft constraints for robust MPC of uncertain systems. *IFAC Proc. Vol.*, 42(11), 225–230.
- Muralidharan, G., Recke, B., Chidambaram, M., and Jørgensen, J.B. (2010). Application of soft constrained MPC to cement mill circuit. *IFAC Proc. Vol.*, 43, 302–307.
- Muralidharan, G., Recke, B., Chidambaram, M., and Jørgensen, J.B. (2013). Soft constrained based MPC for robust control of a cement grinding circuit. *IFAC Proc. Vol.*, 46(32), 475–480.
- Noshirvani, G., Fatehi, A., Araabi, B., Shirvani, M., and Azizi, M. (2009). Comparison of rotary cement kiln identified models. In *IEEE International Conference on Control and Automation*, 1290–1295.
- Ramsamy, V., Kannan, R., Muralidharan, G., Sidharthan, R.K., Veerasamy, G., Venkatesh, S., and Amirtharajan, R. (2023). A comprehensive review on advanced process control of cement kiln processes with the focus on mpc tuning strategies. *J. Process Control*, 121, 85–102.
- Skogestad, S. and Postlethwaite, I. (2005). *Multivariable Feedback Control: Analysis and Design*. Wiley.
- Skogestad, S. (2003). Simple analytic rules for model reduction and pid controller tuning. *J. Process Control*, 13(4), 291–309.
- Spang, H.A. (1972). A dynamic model of a cement kiln. *Automatica*, 8(3), 309–323.
- Stadler, K.S., Poland, J., and Gallestey, E. (2011). Model predictive control of a rotary cement kiln. *Control Engineering Practice*, 19, 1–9.
- Svensen, J.L., Cantisani, N., Da Silva, W.R.L., Pigazo Merino, J., Sampath, D., and Jørgensen, J.B. (2025a). A first engineering principles model for dynamical simulation of cement pyro-process cyclones. In *2025 European Control Conference*, 1346–1351.
- Svensen, J.L., da Silva, W.R.L., and Jørgensen, J.B. (2024a). A first-engineering principles model for dynamical simulation of a calciner in cement production. In *12th IFAC Symposium on Advanced Control of Chemical Processes (ADCHEM 2024)*, 1–7.
- Svensen, J.L., da Silva, W.R.L., Merino, J.P., Sampath, D., and Jørgensen, J.B. (2024b). A dynamical simulation model of a cement clinker rotary kiln. In *2024 European Control Conference*, 1–7.
- Svensen, J.L., Da Silva, W.R.L., Merino, J.P., Sampath, D., and Jørgensen, J.B. (2025b). A dynamic cooler model for cement clinker production. In *2025 European Control Conference*, 2888–2893.
- Svensen, J.L., da Silva, W.R.L., Zhang, Z., Hørsholt, S., and Jørgensen, J.B. (2025c). Dynamical simulation model of the pyro-process in cement clinker production. URL <https://arxiv.org/abs/2504.02886>.
- Teja, R., P., S., and Muralidharan, G. (2016). Control and optimization of a triple string rotary cement kiln using model predictive control. *IFAC-PapersOnLine*, 49-1, 748–753.
- Varnier, L., d’Amore, F., Clausen, K., Melitos, G., de Groot, B., and Bezzo, F. (2025). Combined electrification and carbon capture for low-carbon cement: Techno-economic assessment of different designs. *Journal of Cleaner Production*, 498, 145029.
- Westerlund, T. (1981). A digital quality control system for an industrial dry process rotary cement kiln. *IEEE Transactions on Automatic Control*, AC-26(4), 885–890.
- Zanoli, S.M., Pepe, C., and Rocchi, M. (2015a). Cement rotary kiln: constraints handling and optimization via model predictive control techniques. In *5th Australian Control Conference (AUCC)*, 288–293.
- Zanoli, S.M., Pepe, C., Rocchi, M., and Astolfi, G. (2015b). Application of advanced process control techniques for a cement rotary kiln. In *19th International Conference on System Theory, Control and Computing, ICSTCC 2015 - Joint Conference SINTES 19, SACCS 15, SIMSIS 19*, 723–729.
- Zanoli, S.M., Pepe, C., and Astolfi, G. (2023). Advanced process control for clinker rotary kiln and grate cooler. *Sensors*, 23, 2805.
- Zhang, Z., Nielsen, M.K., Hørsholt, S., Muralidharan, G., and Jørgensen, J.B. (2021). Digitalization, control and optimization for cement plants. In M. Türkay and R. Gani (eds.), *31st European Symposium on Computer Aided Process Engineering*, volume 50 of *Computer Aided Chemical Engineering*, 1319–1324. Elsevier.
- Zhang, Z., Nielsen, M.K., Muralidharan, G., Hørsholt, S., and Jørgensen, J.B. (2022). Model predictive control for blending processes in cement plants. *IFAC-PapersOnLine*, 55(7), 483–488.